Mathematics

http://www.aimspress.com/journal/Math

AIMS Mathematics, 5(6): 5813–5838.
DOI:10.3934/math.2020373
Received: 18 April 2020
Accepted: 20 June 2020
Published: 14 July 2020

Research article

Numerical solution of multi-term time fractional wave diffusion equation using transform based local meshless method and quadrature

Jing Li[1,*], Linlin Dai[2], Kamran[3] and Waqas Nazeer[4]

[1] School of Data Science, Qingdao Huanghai University, Qingdao 266427, China

[2] School of Data Science, Qingdao Huanghai University, Qingdao 266427, China

[3] Department of Mathematics, Islamia College Peshawar, Khyber Pakhtoon Khwa, Pakistan

[4] Department of mathematics, GC University, Lahore Pakistan

* **Correspondence:** Email: lijing811021@163.com.

Abstract: The diffusion equation is a parabolic partial differential equation. In physics, it describes the macroscopic behavior of many micro-particles in Brownian motion, resulting from the random movements and collisions of the particles. In mathematics, it is related to Markov processes, such as random walks, and applied in many other fields, such as materials science, information theory, and biophysics. The present papers deals with the approximation of one and two dimensional multi-term time fractional wave diffusion equations. In this work a numerical method which combines Laplace transform with local radial basis functions method is presented. The Laplace transform eliminates the time variable with which the classical time stepping procedure is avoided, because in time stepping methods the accuracy is achieved at a very small step size, and these methods face sever stability restrictions. For spatial discretization the local meshless method is employed to circumvent the issue of shape parameter sensitivity and ill-conditioning of collocation matrices in global meshless methods. The bounds of the stability for the differentiation matrix of our numerical scheme are derived. The method is tested and validated against 1D and 2D wave diffusion equations. The 2D equations are solved over rectangular, circular and complex domains. The computational results insures the stability, accuracy, and efficiency of the method.

Keywords: Laplace transform; multi-term time fractional wave-diffusion equations; local meshless method; stability; convergence
Mathematics Subject Classification: 26A33, 65M12, 65R10, 81Q05

1. Introduction and preliminaries

Recently, partial differential equations (PDEs) with fractional derivatives have gained significant attention of the research community in applied sciences and engineering. Such equations are encountered in various applications (continuum mechanics, gas dynamics, hydrodynamics, heat and mass transfer, wave theory, acoustics, multiphase flows, chemical engineering, etc.). Numerous phenomenon in Chemistry, Physics, Biology, Finance, Economics and other relevant fields can be modelled using PDEs of fractional order [1–5]. In literature a significant theoretical work on the explicit solution of fractional order differential equations can be found [6, 7] and there references. Since the explicit solutions can be obtained for special cases and most of the time the exact/analytical solutions are cumbersome for differential equations of non-integer order, therefore an alternative way is to find the solutions numerically. Various computational methods have been developed for approximation of differential equations of fractional order. The authors in [8], for example, have analyzed the implicit finite difference method and proved its unconditional convergence and stability. In [9] approximate solution of fractional diffusion equation is obtained via compact finite difference scheme. Liu et al. [10] studied the sub-diffusion equation having non-linear source term using analytical and numerical techniques. In [11] a numerical scheme for the solution of turbulent Riesz type diffusion equation is presented. The authors in [12] have solved diffusion-wave equations of fractional order using a compact finite difference method which is based on its equivalent integro-differential form. Garg et al. [13] utilized the matrix method for approximation of space-time wave-diffusion equation of non-integer order. In [14] the authors solved multi-term wave-diffusion equation of fractional order via Galerkin spectral method and a high order difference scheme. Two finite difference methods for approximating wave-diffusion equations are proposed in [15]. Bhrawy et al. [16] utilized Jacobi operational matrix based spectral tau algorithm for numerical solution of diffusion-wave equation of non-integer order. In [4] the authors proposed numerical schemes for approximating the multi-term wave-diffusion equation. The Legendre wavelets scheme for diffusion wave equations is proposed in [17]. The authors [18] presented a numerical scheme which is based on alternating direction implicit method and compact difference method for 2-D wave-diffusion equations. Similarly a compact difference scheme [19] is utilized for approximation of 1-D and 2-D diffusion-wave equations. Yang et al. [20] proposed a fractional multi-step method for the approximation of wave-diffusion equation of non-integer order. A spectral collocation method and its convergence analysis are presented in [21] for fractional wave-diffusion equation.

Since all these methods are mesh dependent and in modern problems these methods have been facing difficulties due to complicated geometries. Meshfree methods, as an alternative numerical method have attracted the researchers. Some meshless methods have been devoloped such as element-free Galerkin method(EFG) [22], reproducing kernel particle method (RKPM) [23], singular boundary method [24],the boundary particle method [25], Local radial point interpolation method (MLRPI) [26] and so on.

Numerous meshless methods have been developed for the approximation of fractional PDEs. Dehghan et al. [27] analyzed a meshless scheme for approximation of diffusion-wave equation of non-integer order and proved its stability and convergence. In [28] the authors presented an implicit meshless scheme for approximation of anomalous sub-diffusion equation. Diffusion equations of fractional orders are apprximated via RBF based implicit meshless method in [29]. Hosseini et al. [26] developed a local radial point interpolation meshless method based on the Galerkin weak form for numerical solution of wave-diffusion equation of non integer order. In [30] the authors approximated distributed order diffusion-wave equation of fractional order using meshless method. The authors in [31] proposed a meshless point collocation method for approximation of $2-D$ multi-term wave-diffusion equations. In [32] the authors proposed a local meshless method for time fractional diffusion-wave equation. Kansa method [33] is utilized for numerical solution of fractional diffusion equations. Zhuang et al. [34] proposed an implicit MLS meshless method for time fractional advection diffusion equation. The numerical solution of $2D$ wave-diffusion equation is studied in [35] using implicit MLS meshless method. The mentioned methods are meshfree time stepping methods and these methods faces stability restriction in time, and in these methods for convergence a very small step size is required. To overcome the issue of time instability some transformations may be used.

In literature some valuable work is available on resolving the problem of time instability. The researchers have coupled the Laplace transform with other well known numerical methods. For example the Laplace transform with Kansa method [33, 36], finite element method [37, 38], finite difference method [39], RBF method on unit sphere [40] and the references therein. In the present work we have coupled the Laplace transform with local meshless method for approximating the solution of the multi-term diffusion wave equation of fractional order.

2. Laplace transform based local meshless method

In our numerical scheme we transform the multi-term time fractional wave-diffusion equation to a time independent problem with Laplace transformation. The reduced problem is then approximated using local meshless method in Laplace space. Finally the solution of the original problem is obtained using contour integration. We apply the proposed method to multi-term fractional wave-diffusion equation of the form [14]

$$\mathcal{P}_{\alpha,\alpha_1,\alpha_2,\ldots,\alpha_m}(D_\tau)\mathcal{U}(\chi,\tau) = \mathcal{K}\mathcal{L}\mathcal{U}(\chi,\tau) + f(\chi,\tau), \text{ for } \chi \in \Omega,\ \mathcal{K} \in \mathbb{R}\ \ \tau > 0, \tag{2.1}$$

where

$$\mathcal{P}_{\alpha,\alpha_1,\alpha_2,\ldots,\alpha_m}(D_\tau) = D_\tau^\alpha + \sum_{j=1}^{m} d_j D_\tau^{\alpha_j},$$

$1 < \alpha_m < \ldots < \alpha_1 < \alpha < 2$, and $d_j \geq 0$, $j = 1, 2, \ldots, m,\ m \in \mathbb{N}$ are constants. $D_\tau^{\alpha_j}$ is a Caputo derivative of order α_j defined by

$$D_\tau^{\alpha_j} f(\tau) = \frac{1}{\Gamma(n-\alpha_j)} \int_a^\tau \frac{f^{(n)}(\nu)d\nu}{(\tau-\nu)^{\alpha_j+1-n}}, \text{ for } n-1 < \alpha_j < n,\ \ n \in \mathbb{N}, \tag{2.2}$$

also for $n = 2$, we have

$$D_\tau^{\alpha_j} f(\tau) = \frac{1}{\Gamma(n-\alpha_j)} \int_a^\tau \frac{\partial^2 f(\nu)}{\partial \nu^2} \frac{d\nu}{(\tau-\nu)^{\alpha_j-1}}, \text{ for } \alpha_j \in (1,2). \tag{2.3}$$

The initial conditions for the above Eq (2.1) are

$$\mathcal{U}(\chi,0)=\mathcal{U}_0(\chi),\ \ \frac{\partial\mathcal{U}(\chi,0)}{\partial\tau}=\mathcal{U}_1(\chi). \tag{2.4}$$

and the boundary conditions are

$$\mathcal{B}\mathcal{U}(\chi,\tau)=q(\chi,\tau),\ \chi\in\partial\Omega, \tag{2.5}$$

where $\mathcal{L}$ is the governing linear differential operator, and $\mathcal{B}$ is the boundary differential operator. By applying the Laplace transformation to Eq (2.1), we get

$$\hat{\mathcal{U}}(\chi,s)=W(s;\mathcal{L})\hat{g}(\chi,s), \tag{2.6}$$

where

$$W(s;\mathcal{L})=(s^{\alpha}I+s^{\alpha_1}I+...+s^{\alpha_m}I-\mathcal{K}\mathcal{L})^{-1},$$

and

$$\hat{g}(\chi,s)=s^{\alpha-1}\mathcal{U}_0(\chi)+s^{\alpha-2}\mathcal{U}_1(\chi)+s^{\alpha_1-1}\mathcal{U}_0(\chi)+s^{\alpha_1-2}\mathcal{U}_1(\chi)+...+s^{\alpha_m-1}\mathcal{U}_0(\chi)+s^{\alpha_m-2}\mathcal{U}_1(\chi)+\hat{f}(\chi,s).$$

Similarly applying the Laplace transform to (2.5), we get

$$\mathcal{B}\hat{\mathcal{U}}(\chi,s)=\hat{q}(\chi,s), \tag{2.7}$$

Hence, the system of time-independent equations is obtained as

$$\hat{\mathcal{U}}(\chi,s)=W(s;\mathcal{L})\hat{g}(\chi,s), \tag{2.8}$$

$$\mathcal{B}\hat{\mathcal{U}}(\chi,s)=\hat{q}(\chi,s), \tag{2.9}$$

In our method first we represent the solution $\mathcal{U}(\chi,\tau)$ of the original problem (2.1) as a contour integral

$$\mathcal{U}(\chi,\tau)=\frac{1}{2\pi i}\int_{\Gamma}e^{s\tau}\hat{\mathcal{U}}(\chi,s)ds, \tag{2.10}$$

where, for $Res\geq\omega$ with ω appropriately large, and Γ is an initially appropriately chosen line Γ_0 perpendicular to the real axis in the complex plane, with $Ims\to\pm\infty$. The integral (2.10) is just the inverse transform of $\hat{\mathcal{U}}(\chi,\tau)$, with the condition that $\hat{\mathcal{U}}(\chi,\tau)$ must be analytic to the right of Γ_0. To make sure the contour of integration remains in the domain of analyticity of $\hat{\mathcal{U}}(\chi,\tau)$, we select Γ as a deformed contour in the set $\Sigma_{\phi}^{\Upsilon}=\{s\neq 0:|args|<\phi\}\cup\{0\}$, which behaves as a pair of asymptotes in the left half plane, with $Res\to-\infty$ when $Ims\to\pm\infty$, which force $e^{s\tau}$ to decay towards both ends of Γ. In our work we have used two types of contours, the first contour is the hyperbolic contour Γ_1 due to [38] with parametric representation

$$s(\xi)=\Upsilon+\beth(1-\sin(\eta-\iota\xi)),\ \ \xi\in\mathbb{R},\quad(\Gamma_1) \tag{2.11}$$

where,

$$\beth>0,\ 0<\eta<\phi-\frac{\pi}{2},\ \text{and}\ \Upsilon>0. \tag{2.12}$$

By writing $s = x + \iota y$, we observe that Γ_1 is the left branch of the hyperbola

$$\left(\frac{x - \Upsilon - \daleth}{\daleth \sin\eta}\right)^2 - \left(\frac{y}{\daleth \cos\eta}\right)^2 = 1, \tag{2.13}$$

the asymptotes for (2.13) are $y = \pm(x - \Upsilon - \daleth)\cot\eta$, and x-intercept at $s = \Upsilon + \daleth(1 - \sin\eta)$. The condition (2.12) confirms that Γ_1 lies in the sector $\Sigma_\phi^\Upsilon = \Upsilon + \Sigma_\phi \subset \Sigma_\phi$, and grows into the left half plane. From (2.11) and (2.10), we have the following integral

$$\mathcal{U}(\chi, \tau) = \frac{1}{2\pi i}\int_{-\infty}^{\infty} e^{s(\xi)\tau}\hat{\mathcal{U}}(\chi, s(\xi))\acute{s}(\xi)d\xi. \tag{2.14}$$

Finally to approximate Eq (2.14), the trapezoidal rule with step k is used as

$$\mathcal{U}_k(\chi, \tau) = \frac{k}{2\pi i}\sum_{j=-M}^{M} e^{s_j\tau}\hat{\mathcal{U}}(\chi, s_j)\acute{s}_j, \text{ for } \xi_j = jk, \quad s_j = s(\xi_j), \; s'_j = s'(\xi_j). \tag{2.15}$$

The second contour employed in this work is the Talbot's contour [41], though ignored by many researchers, yet it is one of the best method for numerical inverting the Laplace transform [42]. The authors in [43] have optimized the Talbot's contour for approximating the solution of parabolic PDEs. Other works on Talbot's method can be found in [44, 45] and there references. In our work we have employed the improved Talbot's method [46] for numerical inversion of Laplace transform. The Talbot's contour has parametric representation of the form

$$s(\xi) = \frac{M}{\tau}\theta(\xi), \; \theta(\xi) = -\sigma + \mu\xi\cot(\gamma\xi) + \nu\iota\xi, \; -\pi \le \xi \le \pi, \; (\Gamma_2) \tag{2.16}$$

where the parameters σ, μ, ν, and γ are to be specified by the user. From (2.16) and (2.10) we have

$$\mathcal{U}(\chi, \tau) = \frac{1}{2\pi i}\int_{-\pi}^{\pi} e^{s(\xi)\tau}\hat{\mathcal{U}}(\chi, s(\xi))\acute{s}(\xi)d\xi. \tag{2.17}$$

We use M-panel mid-point rule with uniform spacing $k = \frac{2\pi}{M}$, to approximate the integral (2.17) as

$$\mathcal{U}_k(\chi, \tau) = \frac{1}{Mi}\sum_{j=1}^{M} e^{s_j\tau}\hat{\mathcal{U}}(\chi, s_j)\acute{s}_j, \text{ for } \xi_j = -\pi + (j - \frac{1}{2})k, \quad s_j = s(\xi_j), \; s'_j = s'(\xi_j). \tag{2.18}$$

To obtain the solution $\mathcal{U}_k(\chi, \tau)$, first we must solve system of $2M + 1$ equations given in (2.8) and (2.9) for quadrature points s_j, $|j| \le M$. For this purpose the local meshless method is used to discretize operators $\mathcal{L}$, $\mathcal{B}$.

2.1. Local meshless approximation

Given a set of points $\{\chi_i\}_{i=1}^N$ in $\mathbb{R}^d$, where $d \ge 1$ the approximate function for $\hat{\mathcal{U}}(\chi)$ using local meshless method has the form,

$$\hat{\mathcal{U}}(\chi_i) = \sum_{\chi_j \in \Omega_i} \lambda_j^i \phi(\|\chi_i - \chi_j^i\|), \tag{2.19}$$

where $\boldsymbol{\lambda}^i = \{\lambda_j^i\}_{j=1}^n$ is the expansion coefficients vector, $\phi(r)$ is a kernel function,$r = \|\chi_i - \chi_j\|$ is the distance between the centers χ_i and χ_j. Ω, and Ω_i are global domain and local domains respectively. The sub-domain Ω_i contains the center χ_i, and around it, its n neighboring centers. Thus we obtain $n \times n$ linear systems

$$\begin{pmatrix} \hat{\mathcal{U}}(\chi_1^i) \\ \hat{\mathcal{U}}(\chi_2^i) \\ \cdot \\ \cdot \\ \cdot \\ \hat{\mathcal{U}}(\chi_n^i) \end{pmatrix} = \begin{pmatrix} \phi(\|\chi_1^i - \chi_1^i\|) & \phi(\|\chi_1^i - \chi_2^i\|) & \cdot\ \cdot\ \cdot & \phi(\|\chi_1^i - \chi_n^i\|) \\ \phi(\|\chi_2^i - \chi_1^i\|) & \phi(\|\chi_2^i - \chi_2^i\|) & \cdot\ \cdot\ \cdot & \phi(\|\chi_2^i - \chi_n^i\|) \\ \cdot & \cdot & \cdot & \cdot \\ \cdot & \cdot & \cdot & \cdot \\ \cdot & \cdot & \cdot & \cdot \\ \phi(\|\chi_n^i - \chi_1^i\|) & \phi(\|\chi_n^i - \chi_2^i\|) & \cdot\ \cdot\ \cdot & \phi(\|\chi_n^i - \chi_n^i\|) \end{pmatrix} \begin{pmatrix} \lambda_1^i \\ \lambda_2^i \\ \cdot \\ \cdot \\ \cdot \\ \lambda_n^i \end{pmatrix}, \quad i = 1, 2, ..., N, \tag{2.20}$$

which can be written as,

$$\hat{\boldsymbol{\mathcal{U}}}^i = \Phi^i \boldsymbol{\lambda}^i, \ 1 \leq \ i \ \leq N, \tag{2.21}$$

the matrix Φ^i contains elements in the form $b_{kj}^i = \phi(\|\chi_k^i - \chi_j^i\|)$, where $\chi_k^i, \chi_j^i \in \Omega_i$, the unknowns $\boldsymbol{\lambda}^i = \{\lambda_j^i : j = 1, ..., n\}$ are obtained by solving each of the N systems in (2.21). For the differential operator $\mathcal{L}$ we have the form,

$$\mathcal{L}\hat{\mathcal{U}}(\chi_i) = \sum_{\chi_j \in \Omega_i} \lambda_j^i \mathcal{L}\phi(\|\chi_i - \chi_j^i\|), \tag{2.22}$$

the above Eq (2.22) can be expressed as a dot product

$$\mathcal{L}\hat{\mathcal{U}}(\chi_i) = \boldsymbol{\lambda}^i \cdot \boldsymbol{\nu}^i, \tag{2.23}$$

where $\boldsymbol{\nu}^i$ is a n-row vector and $\boldsymbol{\lambda}^i$ is a n-column vector, entries of the n-column vector $\boldsymbol{\nu}^i$ are given as

$$\boldsymbol{\nu}^i = \mathcal{L}\phi(\|\chi_i - \chi_j^i\|), \ \chi_j^i \in \Omega_i, \tag{2.24}$$

eliminating the co efficient $\boldsymbol{\lambda}^i$ from (2.21), and (2.23) we have the following expression

$$\mathcal{L}\hat{\mathcal{U}}(\chi_i) = \boldsymbol{\nu}^i (\Phi^i)^{-1} \hat{\boldsymbol{\mathcal{U}}}^i = \varpi^i \hat{\boldsymbol{\mathcal{U}}}^i \tag{2.25}$$

where,

$$\varpi^i = \boldsymbol{\nu}^i (\Phi^i)^{-1}, \tag{2.26}$$

thus at each node χ_i the approximation of the operator $\mathcal{L}$ via local meshless method is given as

$$\mathcal{L}\hat{\mathcal{U}} \equiv \mathbf{D}\hat{\boldsymbol{\mathcal{U}}}, \tag{2.27}$$

In (2.27) D is a sparse differentiation matrix obtained via local meshless method as an approximation to $\mathcal{L}$. The matrix D has order $N \times N$, it has n non-zero entries, and $N - n$ zero entries, where N is number of centers in global domain, and n is the number of centers in local domain. The boundary operator $\mathcal{B}$ can be discretized in similar way.

3. Convergence and accuracy

In order to solve the multi-term time fractional diffusion wave equation using our proposed method, the local meshless method and Laplace transformation is used. In our numerical scheme first the Laplace transform is applied to time dependent equation which eliminates the time variable, and this process causes no error. Then the local meshless method is utilized for approximating time independent equation. The error estimate for local meshless method is of order $O(\eta^{\frac{1}{\epsilon h}})$,$0 < \eta < 1$, ϵ is the shape parameter and h is the fill distance. In the process of approximating the integrals (2.14) and (2.17) convergence is achieved at different rates depending on the paths Γ_1, and Γ_2. In approximating the integrals (2.14) and (2.17) the convergence order rely upon on the step k of the quadrature rule and the time domain $[t_0, T]$ for Γ_1. The proof for the order of quadrature error for the path Γ_1 is given in the next theorem.

Theorem 3.1 ([38], Theorem 2.1)**.** *Let $\mathcal{U}(\chi,\tau)$ be the solution of* (2.1) *with $\hat{f}(\chi,\tau)$ analytic in Σ_{ϕ}^{Υ}. Let $\Gamma \subset \Omega_r \subset \Sigma_{\phi}^{\Upsilon}$, and define $b > 0$ by $coshb = \frac{1}{\theta\tau_1 \sin(\eta)}$, where $\tau_1 = \frac{t_0}{T}$, $0 < \tau_0 < T$, $0 < \theta < 1.0$ and let $\beth = \frac{\theta\bar{r}M}{bT}$. Then for Eq* (2.15)*, with $k = \frac{b}{M} \leq \frac{\bar{r}}{log2}$, we have $|\mathcal{U}(\chi,\tau) - \mathcal{U}_k(\chi,\tau)| \leq CQe^{\Upsilon\tau_1} l(\rho_r M)e^{-\mu M}\left(||\mathcal{U}_0|| + ||\hat{f}(\chi,\tau)||_{\Sigma_{\phi}^{\Upsilon}}\right)$, for $\mu = \frac{\bar{r}(1-\theta)}{b}$, $\rho_r = \frac{\theta\bar{r}\tau_1\sin(\eta-r_1)}{b}$,$\bar{r} = 2\pi r_1$, $r_1 > 0$, $\tau_0 \leq \tau \leq T$, $C = C_{\eta,r_1,\beta}$, and $l(x) = max(1, log(\frac{1}{x}))$. Hence the error estimate for the proposed scheme is*

$$error_{est}(\Gamma_1) = |\mathcal{U}(\chi,\tau) - \mathcal{U}_k(\chi,\tau)| = O(l(\rho_r M)e^{-\mu M}).$$

The authors in [46] derived the optimal values of the parameters for the Talbot's contour (Γ_2) defined in (2.16) as given below

$$\sigma = 0.6122,\ \mu = 0.5017,\ \nu = 0.2645,\ \text{and}\ \gamma = 0.6407,$$

with corresponding error estimate as

$$error_{est}(\Gamma_2) = |\mathcal{U}(\chi,\tau) - \mathcal{U}_k(\chi,\tau)| = O(e^{-1.358M}).$$

4. Stability

To investigate the stability of the systems (2.8) and (2.9), we represent the system in discrete form as

$$\mathcal{M}\hat{\mathcal{U}} = \mathfrak{b}, \tag{4.1}$$

the matrix $\mathcal{M}_{N\times N}$ is sparse matrix obtained using local meshless method. For the system (4.1) the constant of stability is defined as

$$C = \sup_{\hat{\mathcal{U}}\neq 0} \frac{||\hat{\mathcal{U}}||}{||\mathcal{M}\hat{\mathcal{U}}||}, \tag{4.2}$$

for any discrete norm $||.||$ defined on R^N the constant C is finite . From (4.2) we may write

$$||\mathcal{M}||^{-1} \leq \frac{||\hat{\mathcal{U}}||}{||\mathcal{M}\hat{\mathcal{U}}||} \leq C, \tag{4.3}$$

Similarly for the pseudoinverse $\mathcal{M}^{\dagger}$ of $\mathcal{M}$, we can write

$$\|\mathcal{M}^{\dagger}\| = \sup_{\mathcal{H}\neq 0} \frac{\|\mathcal{M}^{\dagger}\mathcal{H}\|}{\|\mathcal{H}\|}. \tag{4.4}$$

Thus we have

$$\|\mathcal{M}^{\dagger}\| \geq \sup_{\mathcal{H}=\mathcal{M}\hat{\mathcal{H}}\neq 0} \frac{\|\mathcal{M}^{\dagger}\mathcal{M}\hat{\mathcal{U}}\|}{\|\mathcal{M}\hat{\mathcal{U}}\|} = \sup_{\hat{\mathcal{U}}\neq 0} \frac{\|\hat{\mathcal{U}}\|}{\|\mathcal{M}\hat{\mathcal{U}}\|} = C. \tag{4.5}$$

We can see that Eqs (4.3) and (4.5) confirms the bounds for the stability constant C. Calculating the pseudoinverse for approximating the system (4.1) numerically be quite expansive computationally, but it confirms the stability. The MATLAB's function condest can be used to estimate $\|\mathcal{M}^{-1}\|_{\infty}$ in case of square systems, thus we have

$$C = \frac{condest(\mathcal{M}')}{\|\mathcal{M}\|_{\infty}} \tag{4.6}$$

This work well with less number of computations for our sparse differentiation matrix $\mathcal{M}$. Figure 1(a) shows the bounds for the constant C of our system (2.8) and (2.9) for Problem 1 using the Talbot's contour Γ_2. Selecting $N = 80$, $M = 80$, $n = 15$, and $\alpha = 1.8$, $\alpha_1 = 1.7$, $\alpha_2 = 1.6$, $c = 0.6$ at $\tau = 1$, we have $1.00 \leq C \leq 4.5501$. It is observed that the upper and lower bounds for the stability constant are very small numbers, which guarantees that the proposed local meshless scheme is stable.

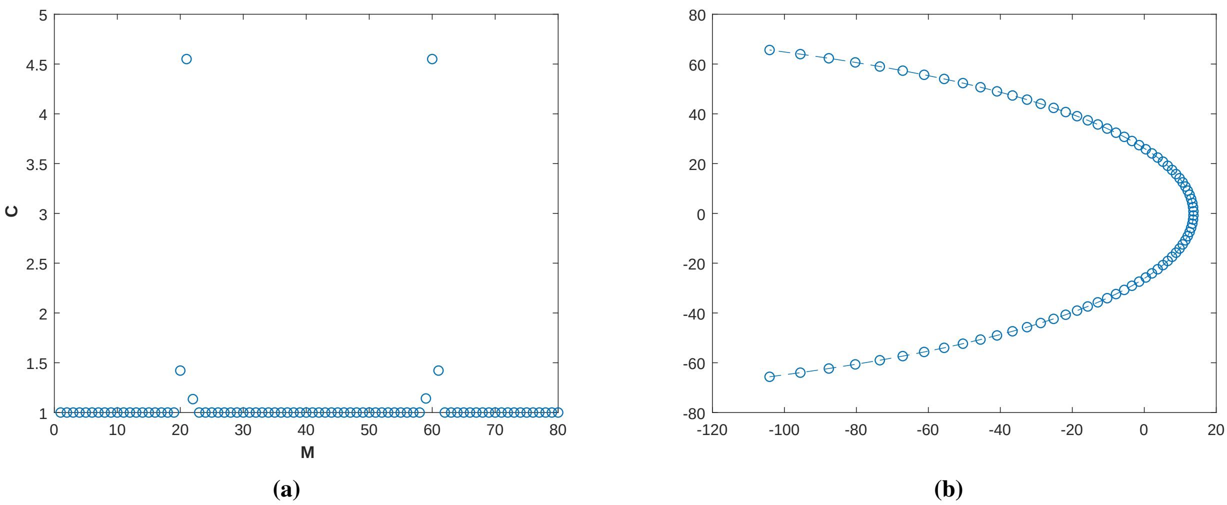

Figure 1. In (a) the plot shows the constant of stability of our proposed method for the matrix $\mathcal{M}$ corresponding to Problem 1, using the Talbot's contour Γ_2. In (b) the Talbot's contour is shown.

5. Numerical results and discussion

The numerical examples are given to validate our proposed Laplace transform based local meshless scheme. In our computations we have considered different $1-D$ and $2-D$ linear multi term wave-diffusion equations. In our numerical examples we have utilized the multi-quadrics(MQ) kernel function $\phi(r,\varepsilon) = (1+(\varepsilon r)^2)^{\frac{1}{2}}$. We have used the uncertainty principal due to [47] for optimization of the shape parameter. The accuracy of the method is measured using L_∞ error defined by

$$L_\infty = \|\mathcal{U}(\chi,\tau) - \mathcal{U}_k(\chi,\tau)\|_\infty = \max_{1\le j\le N}(|\mathcal{U}(\chi,\tau) - \mathcal{U}_k(\chi,\tau)|)$$

is used. Here $\mathcal{U}_k$ and $\mathcal{U}$ are the numerical and exact solutions respectively.

5.1. Problem 1

In the first test problem we consider the following linear fractional equation

$$D_\tau^\alpha \mathcal{U}(\chi,\tau) + D_\tau^{\alpha_1}\mathcal{U}(\chi,\tau) + D_\tau^{\alpha_2}\mathcal{U}(\chi,\tau) - D_\chi^2\mathcal{U}(\chi,\tau) = f(\chi,\tau), \tag{5.1}$$

where

$$\begin{aligned} f(\chi,\tau) = &\left(\frac{6\tau^{3-\alpha}}{\Gamma(4-\alpha)} + \frac{6\tau^{3-\alpha_1}}{\Gamma(4-\alpha_1)} + \frac{6\tau^{3-\alpha_2}}{\Gamma(4-\alpha_2)}\right)\frac{1}{\cosh(\chi-c)} \\ &- \left(\frac{2\tau^3}{cosech(c-\chi)^2\cosh(c-\chi)^3} - \frac{\tau^3}{\cosh(c-\chi)}\right). \end{aligned}$$

The exact solution of the problem is

$$\mathcal{U}(\chi,\tau) = \frac{\tau^3}{\cosh(\chi-c)}, \; c \in \mathbb{R}.$$

The boundary and initial conditions are

$$\mathcal{U}(-10,\tau) = \frac{\tau^3}{\cosh(-10-c)}, \; \mathcal{U}(10,\tau) = \frac{\tau^3}{\cosh(10-c)}, \tag{5.2}$$

and

$$\mathcal{U}_0(\chi) = \mathcal{U}_1(\chi) = 0. \tag{5.3}$$

The points along the hyperbolic contour Γ_1 are calculated using the statement $\xi = -M : k : M$, and along Talbot's contour Γ_2 using the relation $\xi_j = -\pi + (j - \frac{1}{2})k$, where $j = 1 : M$, and $k = \frac{2\pi}{M}$. The parameters used in our computations for the contour Γ_1 are $\theta = 0.10$, $\eta = 0.15410$, $\tau_1 = \frac{t_0}{T}$, $r_1 = 0.13870$, $\bar{r} = 2r_1\pi$, $\Upsilon = 2.0$ The results obtained for the parameters α, α_1, α_2, and c along the contour Γ_1 are displayed in Table 1, and along Γ_2 are displayed in Table 2. The exact and numerical spacetime solutions for the given problem is depicted in Figure 2(a) and in Figure 2(b) respectively. The absolute error and error estimate are displayed in Figure 3(a). Figure 3(b) shows error functions for various values of α_j. The results confirms that our numerical scheme is accurate, stable and can solve multi-term time fractional wave-diffusion equations with less computation time.

Table 1. Numerical solution in the domain [0, 1] and $\tau = 1$ obtained using hyperbolic contour Γ_1.

			$\alpha = 1.5$,	$\alpha_1 = 1.4$,	$\alpha_2 = 1.3$,	$c = 0.5$	
N	n	M	L_∞	c	κ	$error_{est}(\Gamma_1)$	C.TIME(sec)
80	20	35	7.77×10^{-5}	10.0	$1.13\times10^{+12}$	3.14×10^{-1}	0.343148
		55	7.61×10^{-5}	10.0	$1.13\times10^{+12}$	3.64×10^{-2}	1.222487
		75	7.61×10^{-5}	10.0	$1.13\times10^{+12}$	4.2×10^{-3}	5.000861
		95	7.61×10^{-5}	10.0	$1.13\times10^{+12}$	4.75×10^{-4}	12.067666
		110	7.61×10^{-5}	10.0	$1.13\times10^{+12}$	9.30×10^{-5}	22.244950
40	15	80	5.76×10^{-5}	4.5	$1.37\times10^{+12}$	2.4×10^{-3}	2.034147
50			4.70×10^{-5}	5.7	$1.17\times10^{+12}$	2.4×10^{-3}	3.430185
60			4.32×10^{-5}	6.9	$1.05\times10^{+12}$	2.4×10^{-3}	4.307865
70			9.09×10^{-5}	8.0	$1.24\times10^{+12}$	2.4×10^{-3}	5.308744
80			4.82×10^{-5}	9.2	$1.14\times10^{+12}$	2.4×10^{-3}	6.327198
70	12	90	2.33×10^{-5}	7.3	$1.02\times10^{+12}$	8.18×10^{-4}	8.646889
	15		9.09×10^{-5}	8.0	$1.24\times10^{+12}$	8.18×10^{-4}	8.534781
	18		8.80×10^{-5}	8.5	$1.17\times10^{+12}$	8.18×10^{-4}	8.898832
	21		4.10×10^{-5}	8.8	$1.20\times10^{+12}$	8.18×10^{-4}	8.901062
	24		9.30×10^{-5}	9.0	$1.26\times10^{+12}$	8.18×10^{-4}	8.835825
[14]			4.79×10^{-6}				

Table 2. Numerical solution in the domain [0, 1] and $\tau = 1$ obtained using Talbot's contour Γ_2.

			$\alpha = 1.8$,	$\alpha_1 = 1.7$,	$\alpha_2 = 1.6$,	$c = 0.5$	
N	n	M	L_∞	c	κ	$error_{est}(\Gamma_2)$	C.TIME(sec)
70	12	10	3.51×10^{-1}	7.3	$1.02\times10^{+12}$	2.02×10^{-6}	0.201190
		12	3.98×10^{-2}	7.3	$1.02\times10^{+12}$	1.47×10^{-7}	0.202626
		14	4.20×10^{-3}	7.3	$1.02\times10^{+12}$	1.06×10^{-8}	0.213661
		16	4.16×10^{-4}	7.3	$1.02\times10^{+12}$	7.76×10^{-10}	0.203777
		18	4.99×10^{-5}	7.3	$1.02\times10^{+12}$	5.64×10^{-11}	0.204327
30	15	20	2.97×10^{-5}	3.4	$1.00\times10^{+12}$	4.10×10^{-12}	0.203400
40			5.99×10^{-5}	4.5	$1.37\times10^{+12}$	4.10×10^{-12}	0.212062
50			4.82×10^{-5}	5.7	$1.17\times10^{+12}$	4.10×10^{-12}	0.210793
70			9.41×10^{-5}	8.0	$1.24\times10^{+12}$	4.10×10^{-12}	0.222508
90			8.14×10^{-5}	10.4	$1.07\times10^{+12}$	4.10×10^{-12}	0.217812
80	12	20	7.56×10^{-5}	8.3	$1.15\times10^{+12}$	4.10×10^{-12}	0.211422
	14		7.53×10^{-5}	9.0	$1.04\times10^{+12}$	4.10×10^{-12}	0.218499
	16		6.68×10^{-5}	9.4	$1.17\times10^{+12}$	4.10×10^{-12}	0.224207
	18		4.87×10^{-5}	9.8	$1.02\times10^{+12}$	4.10×10^{-12}	0.226878
	20		4.67×10^{-5}	10.0	$1.13\times10^{+12}$	4.10×10^{-12}	0.239581
[14]			5.69×10^{-5}				

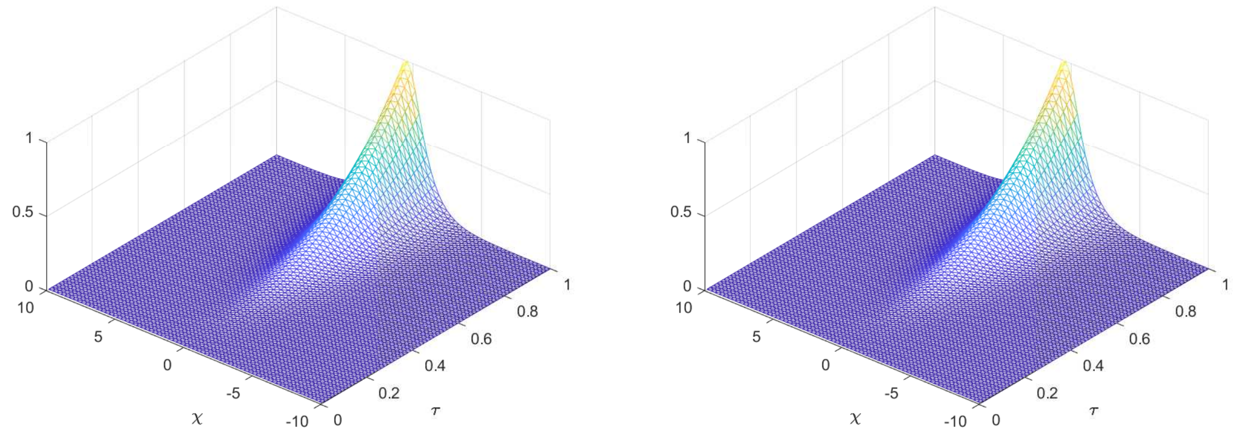

(a) **(b)**

Figure 2. In (a) the spacetime plot shows the exact solutions, in (b) the spacetime plot shows the numerical solution , the parameters used are $\alpha = 1.5$, $\alpha_1 = 1.4$, $\alpha_2 = 1.3$, $c = 0.5$, $N = 70$, $n = 12$, and $M = 90$, along the hyperbolic contour Γ_1.

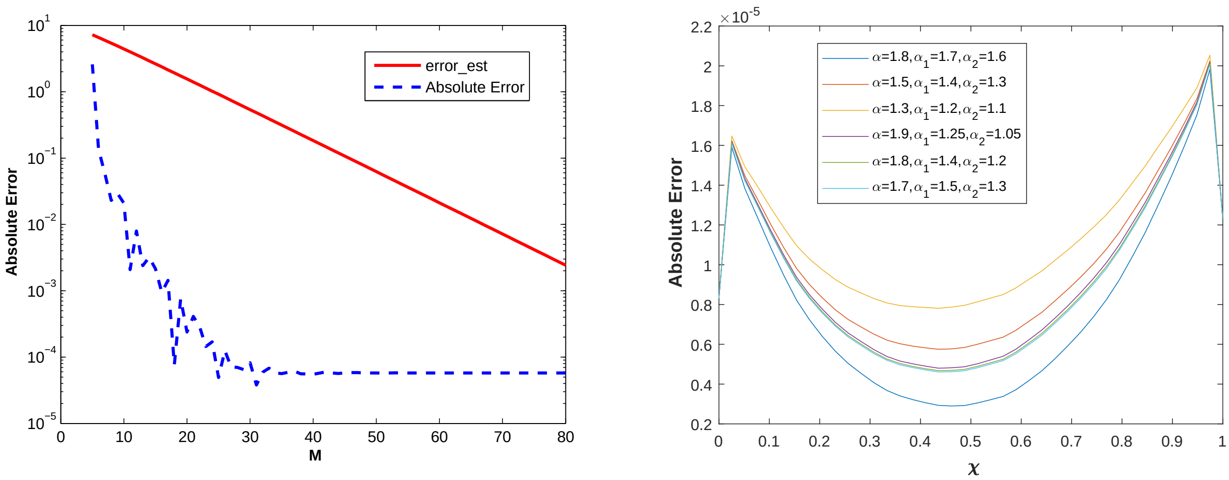

(a) **(b)**

Figure 3. In (a) the Absolute error and error_est(Γ_1) are shown corresponding to problem 1 using $N = 40, n = 15, \alpha = 1.8, \alpha_1 = 1.7, \alpha_2 = 1.6$, $c = 0.5$, the results confirms a good agreement between them. In (b) the error functions for different α, and α_j on $[0, 1]$ are shown using the hyperbolic contour Γ_1.

5.2. *Problem 2*

As a second test problem we consider the following linear fractional equation

$$D_\tau^\alpha \mathcal{U}(\chi,\tau) + D_\tau^{\alpha_1}\mathcal{U}(\chi,\tau) - D_\chi^2 \mathcal{U}(\chi,\tau) = f(\chi,\tau), \tag{5.4}$$

where

$$f(\chi,\tau)=\left(\frac{6\tau^{3-\alpha}}{\Gamma(4-\alpha)}+\frac{6\tau^{3-\alpha_1}}{\Gamma(4-\alpha_1)}+\pi^2\tau^3\right)\sin(\pi\chi).$$

The exact solution of the problem is

$$\mathcal{U}(\chi,\tau)=\sin(\pi\chi)\tau^3.$$

This equation is considered on [0, 1] with boundary conditions

$$\mathcal{U}(0,\tau)=\mathcal{U}(1,\tau)=0 \tag{5.5}$$

and initial conditions

$$\mathcal{U}_0(\chi)=\mathcal{U}_1(\chi)=0. \tag{5.6}$$

In this experiment we have utilized both the contours with the same set of optimal parameters. The numerical experiments are performed with different nodes N in the global domain n in the sub-domain. The results obtained for fractional orders α, and α_1. are displayed in Table 3 along the path Γ_1, and in Table 4 along the path Γ_2. The approximate and exact spacetime solutions are displayed in Figures 4(a) and Figure 4(b). The plot of absolute error and error estimate is displayed in Figure 5(a). Figure 5(b) shows the plot of error functions for various values of α, and α_1. The results verifies the accuracy, stability and efficiency of the proposed local meshless scheme for multi-term time fractional wave-diffusion equations.

Table 3. Numerical solution in the domain [0, 1] and $\tau = 1$ hyperbolic contour Γ_1.

			$\alpha=1.9$,	$\alpha_1=1.3$			
N	n	M	L_∞	c	κ	$error_{est}(\Gamma_1)$	C.TIME(sec)
60	22	40	8.44×10^{-5}	7.6	$1.18\times10^{+12}$	1.83×10^{-1}	0.667872
		60	6.62×10^{-5}	7.6	$1.18\times10^{+12}$	2.12×10^{-2}	1.580686
		80	8.62×10^{-5}	7.6	$1.18\times10^{+12}$	2.4×10^{-3}	7.362587
		90	8.62×10^{-5}	7.6	$1.18\times10^{+12}$	8.18×10^{-4}	10.843996
		100	8.62×10^{-5}	7.6	$1.18\times10^{+12}$	2.76×10^{-4}	15.784191
70	10	100	5.52×10^{-5}	6.4	$1.15\times10^{+12}$	2.76×10^{-4}	17.932164
	12		2.74×10^{-5}	7.3	$1.02\times10^{+12}$	2.76×10^{-4}	17.859075
	14		3.44×10^{-5}	7.8	$1.21\times10^{+12}$	2.76×10^{-4}	18.129870
	18		5.21×10^{-5}	8.5	$1.17\times10^{+12}$	2.76×10^{-4}	18.278882
	22		7.64×10^{-5}	8.9	$1.15\times10^{+12}$	2.76×10^{-3}	18.479720
50	25	90	9.85×10^{-5}	6.5	$1.01\times10^{+12}$	8.18×10^{-4}	8.730629
60			1.03×10^{-4}	7.8	$1.09\times10^{+12}$	8.18×10^{-4}	11.049126
70			5.40×10^{-5}	9.1	$1.14\times10^{+12}$	8.18×10^{-4}	13.349187
80			6.57×10^{-5}	10.4	$1.19\times10^{+12}$	8.18×10^{-4}	15.124607
90			6.17×10^{-5}	11.8	$1.02\times10^{+12}$	8.18×10^{-4}	17.134190
[14]			7.0080×10^{-4}				

Table 4. Numerical solution in the domain [0, 1] and $\tau = 1$ obtained using Talbot's contour Γ_2.

			$\alpha = 1.7,$	$\alpha_1 = 1.2$			
N	n	M	L_∞	c	κ	$error_{est}(\Gamma_2)$	C.TIME(sec)
70	12	10	2.56×10^{-1}	7.3	$1.02\times10^{+12}$	2.02×10^{-6}	0.202184
		12	2.91×10^{-2}	7.3	$1.02\times10^{+12}$	1.47×10^{-7}	0.197720
		14	3.10×10^{-3}	7.3	$1.02\times10^{+12}$	1.06×10^{-8}	0.200589
		16	3.25×10^{-4}	7.3	$1.02\times10^{+12}$	7.76×10^{-10}	0.202710
		18	5.65×10^{-5}	7.3	$1.02\times10^{+12}$	5.64×10^{-11}	0.194221
30	15	20	3.74×10^{-5}	3.4	$1.00\times10^{+12}$	4.10×10^{-12}	0.202098
40			6.97×10^{-5}	4.5	$1.37\times10^{+12}$	4.10×10^{-12}	0.201783
50			6.68×10^{-5}	5.7	$1.17\times10^{+12}$	4.10×10^{-12}	0.204199
70			1.00×10^{-4}	8.0	$1.24\times10^{+12}$	4.10×10^{-12}	0.205864
90			1.36×10^{-4}	10.4	$1.07\times10^{+12}$	4.10×10^{-12}	0.216570
80	12	20	9.70×10^{-5}	8.3	$1.15\times10^{+12}$	4.10×10^{-12}	0.207446
	14		4.34×10^{-5}	9.0	$1.04\times10^{+12}$	4.10×10^{-12}	0.206234
	16		8.47×10^{-5}	9.4	$1.17\times10^{+12}$	4.10×10^{-12}	0.216176
	18		4.76×10^{-5}	9.8	$1.02\times10^{+12}$	4.10×10^{-12}	0.215397
	20		5.66×10^{-5}	10.0	$1.13\times10^{+12}$	4.10×10^{-12}	0.244942
[14]			1.39×10^{-4}				

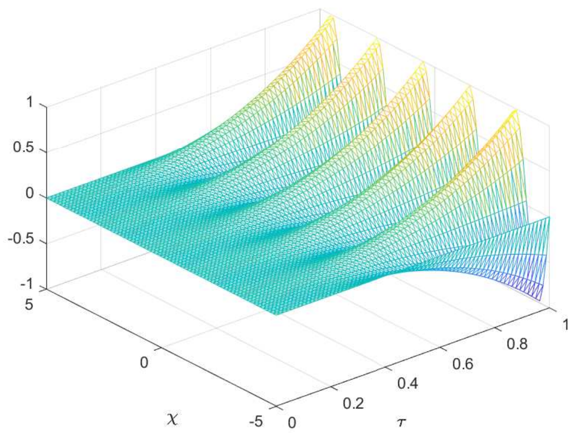

(a)

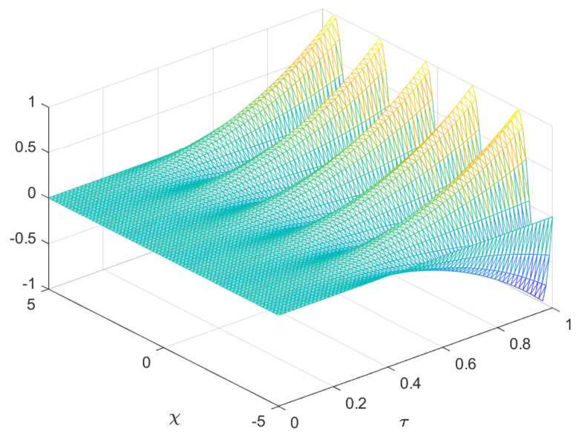

(b)

Figure 4. In (a) The spacetime plot shows the exact solution. In (b) the spacetime plot shows the numerical solution, the parameters used are $\alpha = 1.9$, $\alpha_1 = 1.7$, $N = 70$, $n = 12$, $M = 90$ on $[-5, 5]$, using the hyperbolic contour Γ_1.

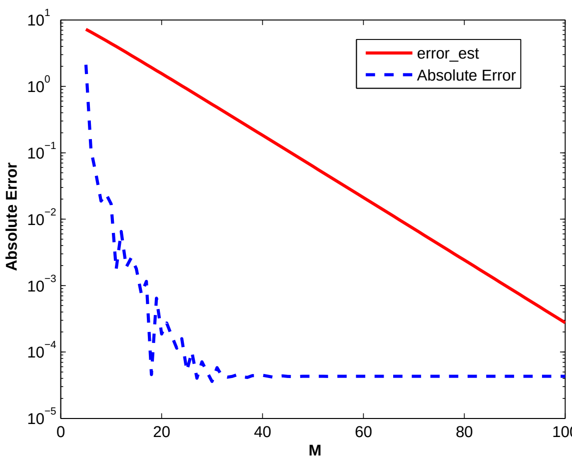

(a)

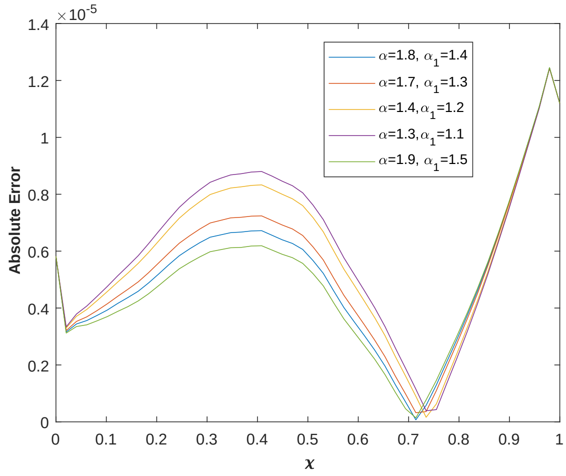

(b)

Figure 5. In (a) Absolute error and error_est for problem 2 are presented using $N = 50, n = 10, \alpha = 1.7, \alpha_1 = 1.2$, the results confirms a good agreement between them. In (b) Error functions for different α, and α_j on $[0, 1]$, are shown using the hyperbolic contour Γ_1. The figure shows that the error decreases with increasing the values of fractional orders α, and α_1.

5.3. Problem 3

We consider the following fractional equation

$$D_\tau^\alpha \mathcal{U}(\chi,\tau) + D_\tau^{\alpha_1}\mathcal{U}(\chi,\tau) - D_\chi^2\mathcal{U}(\chi,\tau) = f(\chi,\tau), \tag{5.7}$$

where

$$f(\chi,\tau) = \left(\frac{2\tau^{2-\alpha}}{\cos(\chi)\Gamma(3-\alpha)} + \frac{2\tau^{2-\alpha_1}}{\cos(\chi)\Gamma(3-\alpha_1)}\right) - \left(\frac{\tau^2}{\cos(\chi)} + \frac{2\tau^2}{cosec(\chi)^2\cos(\chi)^3}\right).$$

The exact solution of the problem is

$$\mathcal{U}(\chi,\tau) = \frac{\tau^2}{\cos(\chi)}.$$

This equation is considered on $[0, 1]$ with boundary conditions

$$\mathcal{U}(0,\tau) = \tau^2,\ \mathcal{U}(1,\tau) = \frac{\tau^2}{\cos(1)} \tag{5.8}$$

and initial conditions

$$\mathcal{U}_0(\chi) = 0,\ \mathcal{U}_1(\chi) = 0. \tag{5.9}$$

The results obtained for third test problem with fractional orders α, and α_1 along the hyperbolic contour Γ_1 are displayed in Tables 5, and along the Talbots contour are displayed in Table 6. From the Tables it can be seen the method has good results in accuracy. Figures 6(a) shows the exact spacetime solution and Figure 6(b) shows the numerical spacetime solution. Figure 7(a), and Figure 7(b) absolute error and error estimate for the contour Γ_1 and Γ_2 respectively .

Table 5. Numerical solution in the domain $[0, 1]$ and $\tau = 1$ hyperbolic contour Γ_1.

			$\alpha = 1.9$,	$\alpha_1 = 1.8$,			
N	n	M	L_∞	c	κ	$error_{est}(\Gamma_1)$	C.TIME(sec)
80	25	50	4.20×10^{-5}	10.4	$1.19\times10^{+12}$	6.25×10^{-2}	2.249386
		60	3.85×10^{-5}	10.4	$1.19\times10^{+12}$	2.12×10^{-2}	4.114330
		70	3.86×10^{-5}	10.4	$1.19\times10^{+12}$	7.2×10^{-3}	7.301508
		90	3.86×10^{-5}	10.4	$1.19\times10^{+12}$	8.18×10^{-4}	15.044453
		100	3.86×10^{-5}	10.4	$1.19\times10^{+12}$	2.76×10^{-4}	21.588645
60	27	90	9.51×10^{-5}	7.9	$1.06\times10^{+12}$	8.18×10^{-4}	11.338375
70			8.41×10^{-5}	9.2	$1.16\times10^{+12}$	8.18×10^{-4}	13.565846
80			1.15×10^{-4}	10.6	$1.01\times10^{+12}$	8.18×10^{-4}	15.034979
90			9.66×10^{-5}	11.9	$1.10\times10^{+12}$	8.18×10^{-4}	17.556509
100			7.93×10^{-5}	13.2	$1.16\times10^{+12}$	8.18×10^{-4}	21.605433
85	20	95	8.45×10^{-5}	10.6	$1.21\times10^{+12}$	4.75×10^{-4}	18.828414
	22		5.73×10^{-5}	10.9	$1.01\times10^{+12}$	4.75×10^{-4}	19.612251
	24		1.68×10^{-4}	11.0	$1.16\times10^{+12}$	4.75×10^{-4}	19.670357
	27		4.26×10^{-5}	11.2	$1.16\times10^{+12}$	4.75×10^{-4}	19.563284
	30		5.36×10^{-5}	11.4	$1.09\times10^{+12}$	4.75×10^{-4}	20.041057
[14]			8.81×10^{-5}				

Table 6. Numerical solution in the domain $[0, 1]$ and $\tau = 1$ obtained using Talbot's contour Γ_2.

			$\alpha = 1.9$,	$\alpha_1 = 1.8$,			
N	n	M	L_∞	c	κ	$error_{est}(\Gamma_2)$	C.TIME(sec)
70	12	10	3.54×10^{-2}	7.3	$1.02\times10^{+12}$	2.02×10^{-6}	0.142848
		12	3.40×10^{-3}	7.3	$1.02\times10^{+12}$	1.47×10^{-7}	0.133224
		14	2.83×10^{-4}	7.3	$1.02\times10^{+12}$	1.06×10^{-8}	0.134380
		16	4.64×10^{-5}	7.3	$1.02\times10^{+12}$	7.76×10^{-10}	0.133445
		18	5.19×10^{-5}	7.3	$1.02\times10^{+12}$	5.64×10^{-11}	0.136420
30	15	20	1.15×10^{-4}	3.4	$1.00\times10^{+12}$	4.10×10^{-12}	0.135380
40			5.10×10^{-5}	4.5	$1.37\times10^{+12}$	4.10×10^{-12}	0.142579
50			1.07×10^{-4}	5.7	$1.17\times10^{+12}$	4.10×10^{-12}	0.137483
70			1.44×10^{-4}	8.0	$1.24\times10^{+12}$	4.10×10^{-12}	0.145392
90			1.49×10^{-4}	10.4	$1.07\times10^{+12}$	4.10×10^{-12}	0.151340
80	12	20	1.29×10^{-4}	8.3	$1.15\times10^{+12}$	4.10×10^{-12}	0.144167
	14		1.22×10^{-4}	9.0	$1.04\times10^{+12}$	4.10×10^{-12}	0.139500
	16		8.31×10^{-5}	9.4	$1.17\times10^{+12}$	4.10×10^{-12}	0.148407
	18		4.78×10^{-5}	9.8	$1.02\times10^{+12}$	4.10×10^{-12}	0.156982
	20		9.51×10^{-5}	10.0	$1.13\times10^{+12}$	4.10×10^{-12}	0.166119
[14]			8.81×10^{-5}				

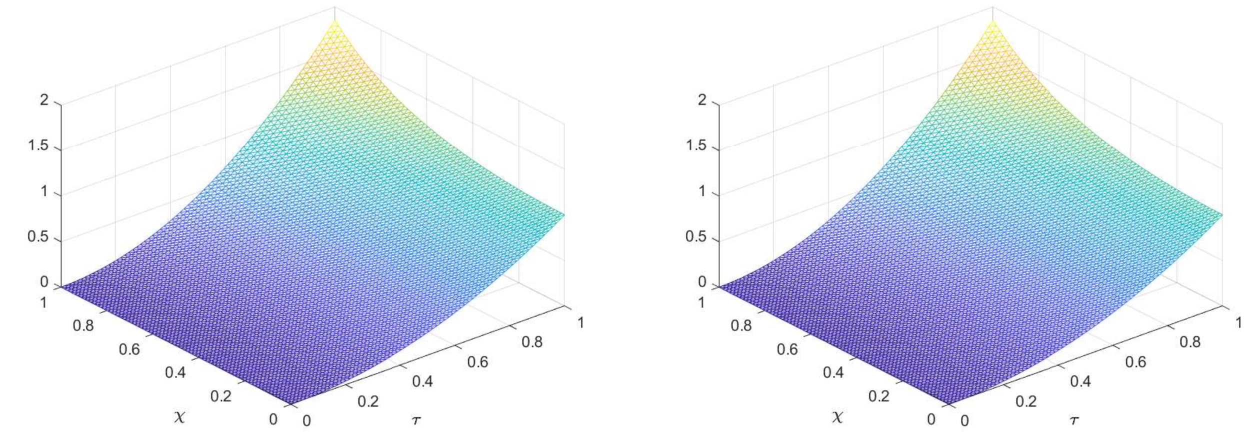

(a) **(b)**

Figure 6. In (a) The spacetime plot shows the exact solution. In (b) The spacetime plot shows the numerical solution, the parameters used are $\alpha = 1.9, \alpha_1 = 1.8,\ N = 70,\ n = 15,\ M = 80$ on $[0, 1]$, using the hyperbolic contour Γ_1.

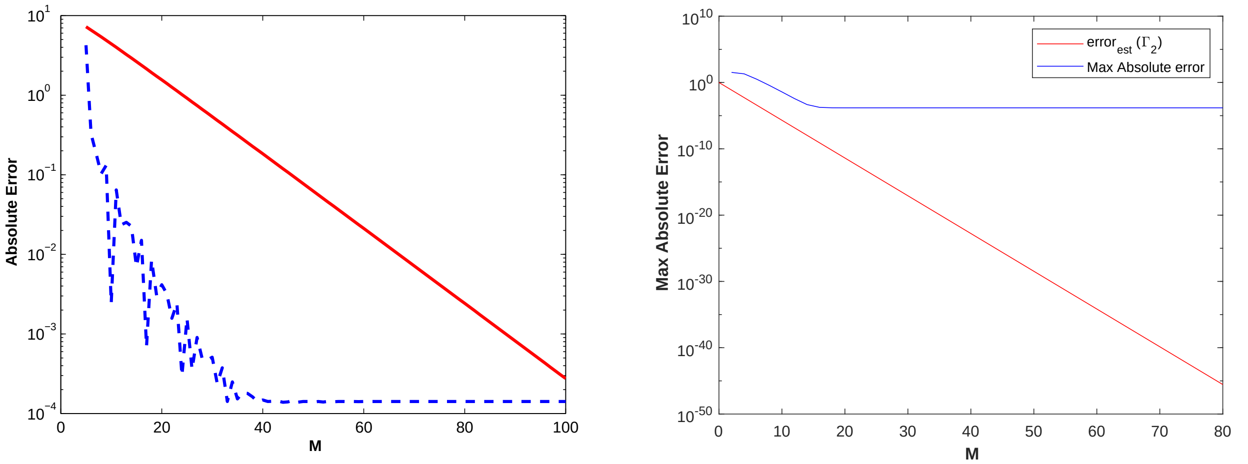

(a) **(b)**

Figure 7. In (a) absolute error and $error_{est}(\Gamma_1)$ are shown corresponding to problem 3 using $N = 50, n = 10, \alpha = 1.9, \alpha_1 = 1.8$, the results confirms a good agreement between them. In (b) absolute error and $error_{est}(\Gamma_2)$ are shown for the parameter values $\alpha = 1.9, \alpha_1 = 1.8,\ N = 70,\ n = 12$ on $[0, 1]$.

5.4. Problem 4

We consider the two dimensional multi-term time fractional wave-diffusion equation

$$D_\tau^\alpha \mathcal{U}(\chi, \vartheta, \tau) + D_\tau^{\alpha_1} \mathcal{U}(\chi, \vartheta, \tau) - \Delta \mathcal{U}(\chi, \vartheta, \tau) = f(\chi, \vartheta, \tau), \tag{5.10}$$

subject to zero initial conditions and the boundary conditions are generated from the exact solution

$$\mathcal{U}(\chi, \vartheta, \tau) = e^{\chi+\vartheta}\tau^{2+\alpha+\alpha_1}$$

the given 2D test problem is solved with regular nodal points in rectangular, circular and complex domains.

5.4.1. Rectangular domain

The rectangular domain $[0, 1]^2$ is descretized with N uniformly distributed points. For this problem also we have used the hyperbolic contour Γ_1 and Talbot's contour Γ_2 with the same set of optimal parameters used for Problem 1. The uniform nodes distribution with boundary stencil red and interior stencil green are shown in Figure 8. The graphs of exact and approximate solutions for the parameters $\alpha = 1.3$, $\alpha_1 = 1.1$, at $\tau = 1$ are shown in the Figure 9(a) and Figure 9(b). The results obtained for various values of N, n, and M along the path Γ_1 and Γ_2 are depicted in Table 7 and Table 8 respectively. From the results one can see that with large number of nodes the proposed method produced accurate results.

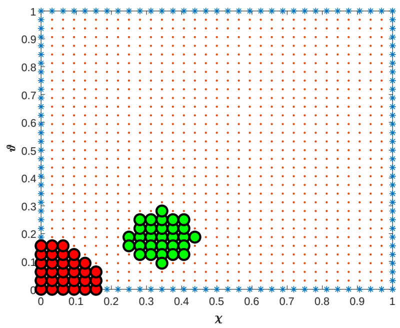

Figure 8. The regular nodes distribution in rectangular domain with boundary stencil red and interior stencil green.

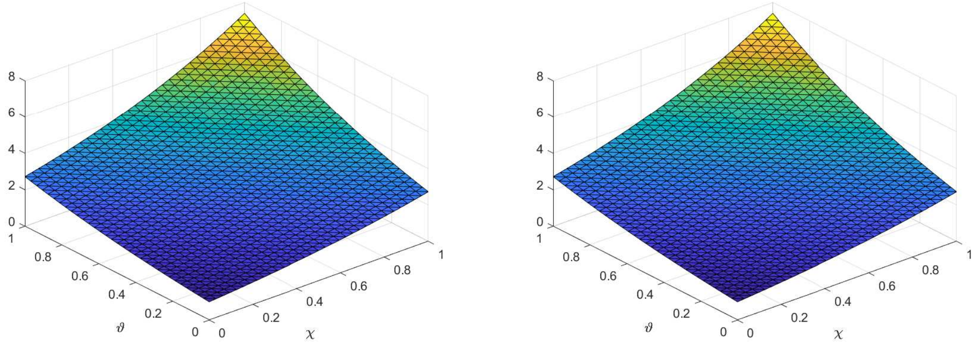

(a) **(b)**

Figure 9. In (a) The plot shows the exact solution. In (b) the plot shows the numerical solution, the parameters used are $\alpha = 1.3$, $\alpha_1 = 1.1$.

Table 7. Numerical solution in the rectangular domain $[0, 1]^2$ for $\alpha = 1.3$, $\alpha_1 = 1.1$, and $\tau = 1$ obtained using hyperbolic contour Γ_1.

			$\alpha = 1.3$,	$\alpha_1 = 1.1$			
N	n	M	L_∞	c	κ	$error_{est}(\Gamma_1)$	C.TIME(sec)
900	14	70	4.26×10^{-2}	1.1	$1.22\times10^{+14}$	7.20×10^{-3}	755.137804
	16		1.12×10^{-2}	1.7	$3.71\times10^{+12}$	7.20×10^{-3}	756.918480
	18		5.00×10^{-3}	1.9	$1.26\times10^{+12}$	7.20×10^{-3}	751.184383
	20		9.22×10^{-4}	2.4	$1.48\times10^{+12}$	7.20×10^{-3}	748.664343
576	20	90	5.15×10^{-4}	1.9	$1.51\times10^{+12}$	8.18×10^{-4}	286.863124
676			5.08×10^{-4}	2.0	$2.19\times10^{+12}$	8.18×10^{-4}	421.440624
784			8.58×10^{-4}	2.2	$1.77\times10^{+12}$	8.18×10^{-4}	608.764593
900			9.22×10^{-4}	2.4	$1.48\times10^{+12}$	8.18×10^{-4}	861.916452
729	20	20	1.10×10^{-3}	2.1	$1.96\times10^{+12}$	$1.55\times10^{+0}$	22.119245
		30	7.80×10^{-4}	2.1	$1.96\times10^{+12}$	5.73×10^{-1}	48.770754
		50	7.57×10^{-4}	2.1	$1.96\times10^{+12}$	6.25×10^{-2}	138.310373
		80	7.57×10^{-4}	2.1	$1.96\times10^{+12}$	2.40×10^{-3}	386.725304

Table 8. Numerical solution in the rectangular domain $[0, 1]^2$ for $\alpha = 1.3$, $\alpha_1 = 1.1$, and $\tau = 1$ obtained using Talbot's contour Γ_2.

			$\alpha = 1.3$,	$\alpha_1 = 1.1$			
N	n	M	L_∞	c	κ	$error_{est}(\Gamma_2)$	C.TIME(sec)
900	20	16	1.98×10^{-1}	2.4	$1.48\times10^{+12}$	7.76×10^{-6}	9.513650
		18	2.15×10^{-2}	2.4	$1.48\times10^{+12}$	5.64×10^{-11}	10.640051
		20	2.00×10^{-3}	2.4	$1.48\times10^{+12}$	4.10×10^{-12}	11.661281
		22	8.40×10^{-4}	2.4	$1.48\times10^{+12}$	2.97×10^{-13}	12.824995
		24	9.12×10^{-4}	2.4	$1.48\times10^{+12}$	2.16×10^{-14}	13.560164
900	14	24	4.28×10^{-2}	1.1	$1.22\times10^{+14}$	2.16×10^{-14}	13.026362
	16		1.12×10^{-2}	1.7	$3.31\times10^{+12}$	2.16×10^{-14}	13.463156
	18		5.00×10^{-3}	1.9	$1.26\times10^{+12}$	2.16×10^{-14}	13.591828
	20		9.12×10^{-4}	2.4	$1.48\times10^{+12}$	2.16×10^{-14}	13.601463
576	20	22	5.11×10^{-4}	1.9	$1.51\times10^{+12}$	2.97×10^{-13}	4.451590
676			5.17×10^{-4}	2.0	$2.19\times10^{+12}$	2.97×10^{-13}	6.401350
784			8.14×10^{-4}	2.2	$1.77\times10^{+12}$	2.97×10^{-13}	9.076440
900			8.40×10^{-4}	2.4	$1.48\times10^{+12}$	2.97×10^{-13}	12.560123
961			8.06×10^{-4}	2.4	$2.19\times10^{+12}$	2.97×10^{-13}	14.919706

5.4.2. Circular Domain

Here we solve the given problem in unit circle with center at $(\chi, \vartheta) = (0.5, 0.5)$. The domain is descretized with N uniform nodes. The computational results for different values of N, n, and M along Γ_1 and Γ_2 are depicted in Table 9 and Table 10 respectively. Figure 10(a) shows the uniform nodes in circular domain, whereas Figure 10(b) shows the absolute error computed along the hyperbolic path.

The exact and approximate solutions are presented in Figures 11(a) and Figure 11(b). The proposed method produced results with good accuracy in circular domain.

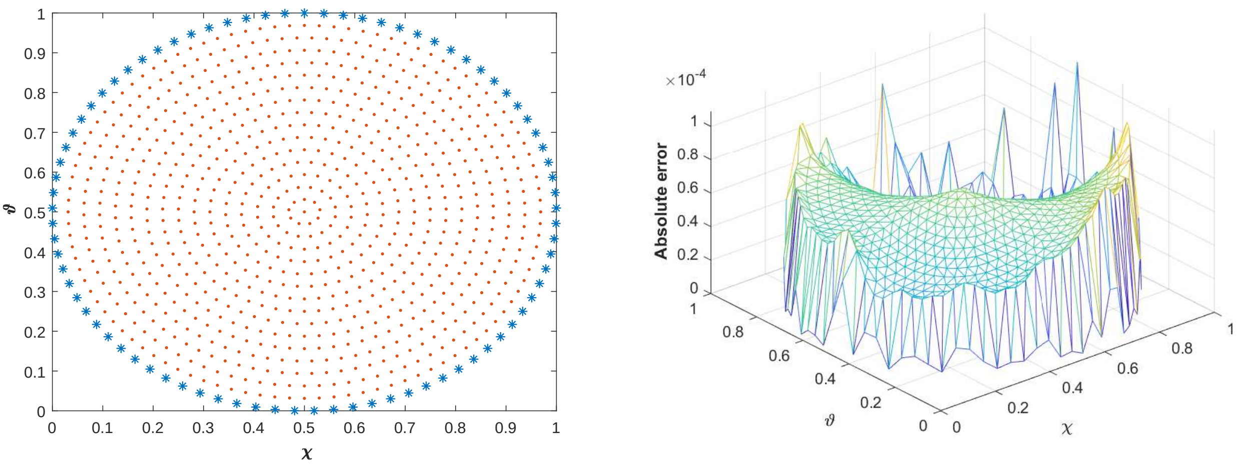

(a) **(b)**

Figure 10. In (a) The regular nodes distribution in circular domain are shown. In (b) the plot shows the absolute error for the parameters values $\alpha = 1.7$, $\alpha_1 = 1.5, N = 900$, $n = 50$, and $M = 90$ along the hyperbolic contour Γ_1.

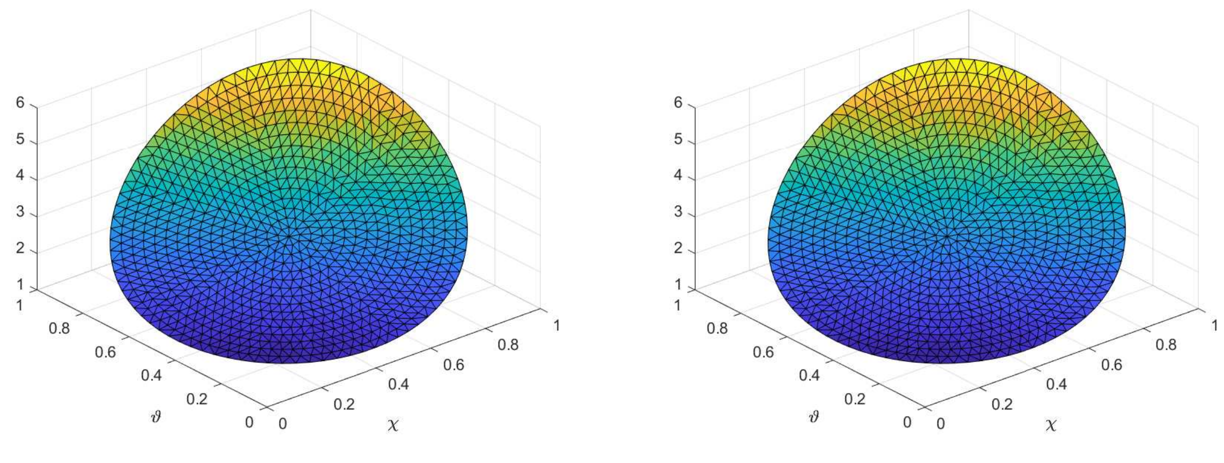

(a) **(b)**

Figure 11. In (a) The plot shows the exact solution. In (b) the plot shows the numerical solution, the parameters used are $\alpha = 1.5$, $\alpha_1 = 1.3$.

Table 9. Numerical solution in the circular domain for $\alpha = 1.3,\ \alpha_1 = 1.1$, and $\tau = 1$ obtained using hyperbolic contour Γ_1.

			$\alpha = 1.3,$	$\alpha_1 = 1.1$			
N	n	M	L_∞	c	κ	$error_{est}(\Gamma_1)$	C.TIME(sec)
950	60	15	8.30×10^{-3}	4.3	$3.11\times10^{+12}$	$2.63\times10^{+0}$	38.116660
		20	1.20×10^{-3}	4.3	$3.11\times10^{+12}$	$1.55\times10^{+0}$	62.890208
		30	9.23×10^{-4}	4.3	$3.11\times10^{+12}$	5.37×10^{-1}	133.694751
		40	9.17×10^{-4}	4.3	$3.11\times10^{+12}$	1.83×10^{-2}	369.149122
900	30	50	1.30×10^{-3}	3.1	$2.82\times10^{+12}$	6.25×10^{-2}	361.783503
	40		2.10×10^{-3}	3.5	$5.12\times10^{+12}$	6.25×10^{-2}	366.883195
	50		2.20×10^{-3}	4.1	$2.43\times10^{+12}$	6.25×10^{-2}	363.312789
	60		9.17×10^{-4}	4.3	$3.11\times10^{+12}$	6.25×10^{-2}	367.839901
300	59	60	9.77×10^{-4}	4.3	$3.06\times10^{+12}$	2.12×10^{-2}	553.852222
550			9.77×10^{-4}	4.3	$3.06\times10^{+12}$	2.12×10^{-2}	447.562447
800			9.77×10^{-4}	4.3	$3.06\times10^{+12}$	2.12×10^{-2}	531.883062
1100			9.77×10^{-4}	4.3	$3.06\times10^{+12}$	2.12×10^{-2}	531.921143

Table 10. Numerical solution in the circular domain for $\alpha = 1.5,\ \alpha_1 = 1.3$, and $\tau = 1$ obtained using Talbot's contour Γ_2.

			$\alpha = 1.5,$	$\alpha_1 = 1.3$			
N	n	M	L_∞	c	κ	$error_{est}(\Gamma_2)$	C.TIME(sec)
950	50	18	5.87×10^{-2}	4.1	$2.43\times10^{+12}$	5.64×10^{-11}	9.258343
		20	7.60×10^{-3}	4.1	$2.43\times10^{+12}$	4.10×10^{-12}	9.959348
		22	2.40×10^{-3}	4.1	$2.43\times10^{+12}$	2.97×10^{-13}	10.597861
		24	1.90×10^{-3}	4.1	$2.43\times10^{+12}$	2.16×10^{-14}	11.241704
1050	10	26	9.43×10^{-2}	1.2	$7.70\times10^{+13}$	1.57×10^{-15}	9.389988
	30		1.20×10^{-3}	3.1	$2.82\times10^{+12}$	1.57×10^{-15}	10.100778
	50		1.90×10^{-3}	4.1	$2.43\times10^{+12}$	1.57×10^{-15}	11.882140
	60		8.84×10^{-4}	4.3	$3.11\times10^{+12}$	1.57×10^{-15}	13.157724
750	59	28	9.36×10^{-4}	4.3	$3.06\times10^{+12}$	1.14×10^{-16}	13.662250
1150			9.36×10^{-4}	4.3	$3.06\times10^{+12}$	1.14×10^{-16}	13.759729
1250			9.36×10^{-4}	4.3	$3.06\times10^{+12}$	1.14×10^{-16}	13.572409

5.4.3. Complex Shape Domain

In the last test problem we have considered the complex shape domain. The domain is generated by $r_d = \frac{1}{d}[1 + 2d + d^2 - (d+1)\cos(d\theta)], d = 4$. In this experiment also we have used the contours Γ_1 and Γ_2 with the same set of optimal parameters used in Problem 1. The results obtained for fractional orders $\alpha = 1.5,\ \alpha_1 = 1.3$, and various nodes N in the global domain and n in the local domain and quadrature points along the contour Γ_1 and Γ_2 are shown in Table 11 and Table 12 respectively. The regular nodes distribution in the complex domain are shown in Figure 12(a), whereas the approximate and exact solutions are presented in Figures 12(b). Figure 13 shows the absolute error obtained using the Talbots contour. It can be seen that the proposed numerical method produced very accurate and stable results in the complex domain, this confirms the efficiency of the method for such type of equations.

Table 11. Numerical solution in the circular domain for $\alpha = 1.5$, $\alpha_1 = 1.3$, and $\tau = 1$ obtained using hyperbolic contour Γ_1.

			$\alpha = 1.5$,	$\alpha_1 = 1.3$			
N	n	M	L_∞	c	κ	$error_{est}(\Gamma_1)$	C.TIME(sec)
851	50	40	4.70×10^{-3}	4.0	$1.13\times10^{+12}$	1.83×10^{-1}	50.524737
		50	6.75×10^{-4}	4.0	$1.13\times10^{+12}$	6.25×10^{-2}	79.388630
		60	6.74×10^{-4}	4.0	$1.13\times10^{+12}$	2.12×10^{-2}	116.511151
		80	6.74×10^{-4}	4.0	$1.13\times10^{+12}$	2.40×10^{-3}	227.719695
852	30	70	1.30×10^{-3}	2.9	$6.40\times10^{+12}$	7.20×10^{-3}	147.655977
	40		1.20×10^{-3}	3.4	$5.83\times10^{+12}$	7.20×10^{-3}	158.960295
	50		9.34×10^{-4}	3.9	$1.82\times10^{+12}$	7.20×10^{-3}	219.043351
	60		9.47×10^{-4}	4.2	$1.92\times10^{+12}$	7.20×10^{-3}	268.501711
457	60	60	6.97×10^{-4}	3.0	$3.07\times10^{+12}$	2.12×10^{-2}	68.420275
542			4.39×10^{-4}	3.3	$1.62\times10^{+12}$	2.12×10^{-2}	89.095051
643			4.86×10^{-4}	3.6	$1.79\times10^{+12}$	2.12×10^{-2}	117.459116
851			7.29×10^{-4}	4.2	$1.90\times10^{+12}$	2.12×10^{-2}	184.241136

Table 12. Numerical solution in the circular domain for $\alpha = 1.5$, $\alpha_1 = 1.3$, and $\tau = 1$ obtained using Talbot's contour Γ_2.

			$\alpha = 1.5$,	$\alpha_1 = 1.3$			
N	n	M	L_∞	c	κ	$error_{est}(\Gamma_2)$	C.TIME(sec)
752	30	24	1.10×10^{-3}	2.7	$3.89\times10^{+12}$	2.16×10^{-14}	3.188624
850			1.80×10^{-3}	2.9	$7.98\times10^{+12}$	2.16×10^{-14}	3.613122
921			1.50×10^{-3}	3.0	$2.48\times10^{+13}$	2.16×10^{-14}	4.028301
974			9.61×10^{-4}	3.2	$5.64\times10^{+12}$	2.16×10^{-14}	4.297978
1020	28	22	2.90×10^{-3}	2.9	$3.79\times10^{+13}$	2.97×10^{-13}	4.261794
	40		1.90×10^{-3}	3.7	$2.62\times10^{+13}$	2.97×10^{-13}	5.485432
	50		1.00×10^{-3}	4.2	$1.13\times10^{+13}$	2.97×10^{-13}	6.750489
	60		9.32×10^{-4}	4.6	$6.25\times10^{+12}$	2.97×10^{-13}	8.366275
1095	70	18	6.47×10^{-2}	5.1	$2.15\times10^{+12}$	5.64×10^{-11}	10.452683
		20	6.60×10^{-3}	5.1	$2.15\times10^{+12}$	4.10×10^{-12}	10.778798
		22	9.01×10^{-4}	5.1	$2.15\times10^{+12}$	2.97×10^{-13}	11.238818
		24	9.97×10^{-4}	5.1	$2.15\times10^{+12}$	2.16×10^{-14}	11.540931

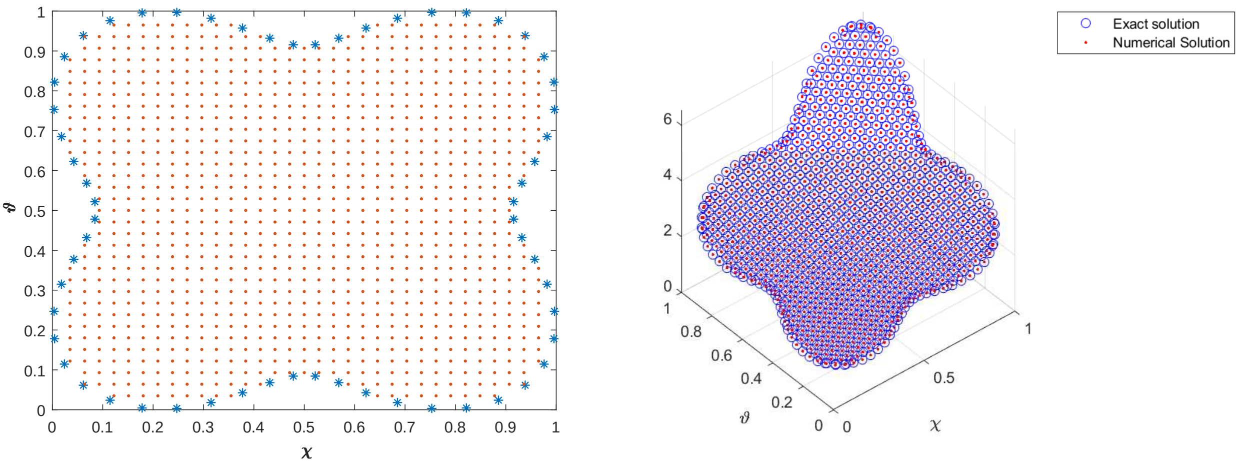

(a) **(b)**

Figure 12. In (a) The regular nodes distribution in complex domain is shown. In (b) the plot shows the numerical solution and exact solutions, the parameters used are $\alpha = 1.5$, $\alpha_1 = 1.3$.

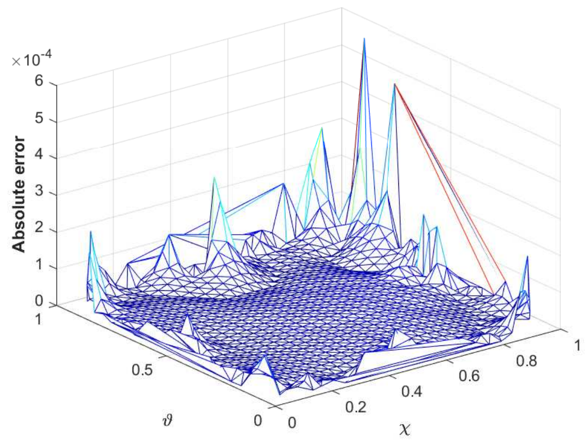

Figure 13. The plot shows absolute error obtained using Talbot's contour Γ_2 for the parameter values $N = 993,\ n = 30,\ M = 24,\ \alpha = 1.5$, and $\alpha_1 = 1.3$, at $\tau = 1$.

6. Conclusion

In this work, a local meshless method based on Laplace transform has been utilized for the approximation of the numerical solution of 1D and 2D multi-term time fractional wave diffusion equations. We resolved the issue of time-instability which is the common short coming of time-stepping methods using the Laplace transformation, and the issues of ill-conditioning due to dense differentiation matrices and shape parameter sensitivity with localized meshless method. The stability and convergence of the method are discussed. To verify the theoretical results some test problem in 1D and a test problem in 2D are considered. For the two dimensional problem we have considered rectangular, circular, and complex domains. For numerical inversion of Laplace transform we have utilized two types of contours the hyperbolic and the improved Talbot's contour. The results obtained using these two contours were accurate and stable. However, the results show that the Talbot's contour is more efficient computationally. The benefit of this method is that it can approximate such type equations very efficiently and accurately with less computation time, and without any time instability. The obtained results proves the simplicity in implementation, efficiency, accuracy, and stability of the proposed method.

Acknowledgment

This work was supported by "the Construction team project of the introduction and cultivation of young innovative talents in Colleges and universities of Shandong Province of China, 2019 (Project Name: Big data and business intelligence social service innovation team)" and "the Social Science Planning Project of Qingdao, China,2018 (Grant No. QDSKL1801229)".

Conflict of interest

The authors declare that no competing interests exist.

First and second authors revised the paper, solved the examples and used software to compute and sketch the results. Third author did analysis and wrote the paper. Forth proposed the problem and verified the results.

References

1. K. Oldham, J. Spanier, *The Fractional Calculus Theory and Applications of Differentiation and Integration to Arbitrary Order*, Elsevier, 1974.
2. F. Mainardi, *Fractional relaxation-oscillation and fractional diffusion-wave phenomena*, Chaos, Soliton. Fract., **7** (1996), 1461–1477.
3. A. Carpinteri , F. Mainardi, *Fractals and Fractional Calculas Continuum Mechanics*, Springer-Verlag Wien, 1997.
4. F. Liu, M. M. Meerschaert, R. J. McGough, et al. *Numerical methods for solving the multi-term time-fractional wave-diffusion equation*, Fract. Calc. Appl. Anal., **16** (2013), 9–25.
5. H. Ding, C. Li, *Numerical algorithms for the fractional diffusion-wave equation with reaction term*, Abstr. Appl. Anal., **2013** (2013), 1–15.
6. K. Diethelm, N. J. Ford, *Analysis of fractional differential equations*, J. Math. Anal. Appl., **265** (2002), 229–248.
7. H. Ye, F. Liu, V. Anh, et al. *Maximum principle and numerical method for the multi-term time-space riesz-caputo fractional differential equations*, Appl. Math. Model., **227** (2014), 531–540.
8. C. M. Chen, F. Liu, I. Turner, et al. *A fourier method for the fractional diffusion equation describing sub-diffusion*, J. Comput. Phys., **227** (2007), 886–897.
9. M. Cui, *Compact finite difference method for the fractional diffusion equation*, J. Comput. Phys., **228** (2009), 7792–7804.

10. F. Liu, C. Yang, K. Burrage, *Numerical method and analytical technique of the modified anomalous subdiffusion equation with a nonlinear source term*, J. Comput. Appl. Math., **231** (2009), 160–176.
11. H. Ding, C. Li, *High-order numerical methods for riesz space fractional turbulent diffusion equation*, Fract. Calc. Appl. Anal., **19** (2016), 19–55.
12. A. Chen, C. Li, *Numerical solution of fractional diffusion-wave equation*, Numer. Func. Anal. Opt., **37** (2016), 19–39.
13. M. Garg, P. Manohar, *Numerical solution of fractional diffusion-wave equation with two space variables by matrix method*, Fract. Calc. Appl. Anal., **13** (2010), 191–207.
14. M. Dehghan, M. Safarpoor, M. Abbaszadeh, *Two high-order numerical algorithms for solving the multi-term time fractional diffusion-wave equations*, J. Comput. Appl. Math., **290** (2015), 174–195.
15. J. Huang, Y. Tang, L. Vázquez, et al. *Two finite difference schemes for time fractional diffusion-wave equation*, Numer. Algorithms, **64** (2013), 707–720.
16. A. H. Bhrawy, E. H. Doha, D. Baleanu, et al. *A spectral tau algorithm based on jacobi operational matrix for numerical solution of time fractional diffusion-wave equations*, J. Comput. Phys., **293** (2015), 142–156.
17. M. H. Heydari, M. R. Hooshmandasl, F. M. M. Ghaini, et al, *Wavelets method for the time fractional diffusion-wave equation*, Phys. Lett. A, **379** (2015), 71–76.
18. Y. N. Zhang, Z. Z. Sun, X. Zhao, *Compact alternating direction implicit scheme for the two-dimensional fractional diffusion-wave equation*, SIAM J. Numer. Anal., **50** (2012),1535–1555.
19. J. Ren, Z. Z. Sun, *Efficient numerical solution of the multi-term time fractional diffusion-wave equation*, E. Asian J. Appl. Math., **5** (2015),1–28.
20. J. Y. Yang, J. F. Huang, D. M.Liang, et al. *Numerical solution of fractional diffusion-wave equation based on fractional multistep method*, Appl. Math. Model., **38** (2014), 3652–3661.
21. Y. Yang, Y. Chen, Y. Huang, et al. *Spectral collocation method for the time-fractional diffusion-wave equation and convergence analysis*, Comput. Math. Appl., **73** (2017), 1218–1232.
22. T. Belytschko, Y. Y. Lu, L. Gu, *Element free galerkin methods*, Int. J. Numer. Meth. Eng., **37** (1994), 229–256.
23. W. K. Liu, Y. Chen, S. Jun, et al. *Overview and applications of the reproducing kernel particle methods*, Arch. Comput. Method. E., **3** (1996), 3–80.
24. W. Chen, *Singular boundary method: a novel, simple, meshfree, boundary collocation numerical method*, Chin. J. Solid Mech., **30** (2009), 592–599.
25. Z. Fu, W. Chen, C. Zhang, *Boundary particle method for cauchy inhomogeneous potential problems*, Inverse probl. Sci. En., **20** (2012), 189–207.
26. V. R. Hosseini, E. Shivanian, W. Chen, *Local radial point interpolation (MLRPI) method for solving time fractional diffusion-wave equation with damping*, J. Comput. Phys., **312** (2016), 307–332.
27. M. Dehghan, M. Abbaszadeh, A. Mohebbi, *Analysis of a meshless method for the time fractional diffusion-wave equation*, Numer. algorithms, **73** (2016), 445–476.

28. Y. Gu, P. Zhuang, F. Liu, *An advanced implicit meshless approach for the non-linear anomalous subdiffusion equation*, CMES-Comp. Model. Eng., **56** (2010), 303–334.

29. Q. Liu, Y. T. Gu, P. Zhuang, et al. *An implicit rbf meshless approach for time fractional diffusion equations*, Comput. Mech., **48** (2011), 1–12.

30. M. Abbaszadeh, M. Dehghan, *An improved meshless method for solving two-dimensional distributed order time-fractional diffusion-wave equation with error estimate*, Numer. Algorithms, **75** (2017), 173–211.

31. R. Salehi, *A meshless point collocation method for 2-d multi-term time fractional diffusion-wave equation*, Numer. Algorithms, **74** (2017), 1145–1168.

32. M. Uddin, Kamran, A. Ali, *A localized transform-based meshless method for solving time fractional wave-diffusion equation*, Eng. Anal. Bound. Elem., **92** (2018), 108–113.

33. W. Chen, L. Ye, H. Sun, *Fractional diffusion equations by the kansa method*, Comput. Math. Appl., **59** (2010), 1614–1620.

34. P. Zhuang, Y. T. Gu, F. Liu, et al. *Time-dependent fractional advection–diffusion equations by an implicit mls meshless method*, Int. J. Numer. Meth. Eng., **88** (2011), 1346–1362.

35. J. Y. Yang, Y. M. Zhao, N. Liu, et al. *An implicit mls meshless method for 2-d time dependent fractional diffusion–wave equation*, Appl. Math. Model., **39** (2015), 1229–1240.

36. G. J. Moridis, E. J. Kansa, *The Laplace transform multiquadric method: a highly accurate scheme for the numerical solution of partial differential equations*, J. Appl. sci. comput., **1** (1994) 375–475.

37. W. McLean, V. Thomee, *Time discretization of an evolution equation via laplace transforms*, IMA J. Numer. Anal., **24** (2004), 439 –463.

38. W. McLean, V. Thomée, *Numerical solution via laplace transforms of a fractional order evolution equation*, J. Integral Equ. Appl., **22** (2010), 57–94.

39. B. A. Jacobs, *High-order compact finite difference and Laplace transform method for the solution of time fractional heat equations with Dirichlet and Neumann boundary conditions*, Numer. Meth. Part. D. E., **32** (2016), 1184–1199.

40. Q. T. L. Gia, W. Mclean, *Solving the heat equation on the unit sphere via Laplace transforms and radial basis functions*, Adv. Comput. Math., **40** (2014), 353–375.

41. A. Talbot, *The accurate numerical inversion of laplace transform*, IMA J. Appl. Math., **23** (1979), 97–120.

42. D. G. Duffy, *On the numerical inversion of laplace transforms: comparison of three new methods on characteristic problems from applications*, ACM T. Math. Software, **19** (1993), 333–359.

43. J. A. C. Weideman, *Optimizing talbot's contours for the inversion of the laplace transform*, SIAM J. Numer. Anal., **44** (2006), 2342–2362.

44. C. Lubich, A. Schädle, *Fast convolution for nonreflecting boundary conditions*, SIAM J. Sci. Comput., **24** (2002), 161–182.

45. F. Zeng, I. Turner, K. Burrage, et al. *A new class of semi-implicit methods with linear complexity for nonlinear fractional differential equations*, SIAM J. Sci. Comput., **40** (2018), A2986–A3011.

46. B. Dingfelder, J. Weideman, *An improved talbot method for numerical laplace transform inversion*, Numer. Algorithms, **68** (2015), 167–183.

47. R. Schaback, *Error estimates and condition numbers for radial basis function interpolation*, Adv. Comput. Math., **3** (1995), 251–264.

AIMS Press

© 2020 the Author(s), licensee AIMS Press. This is an open access article distributed under the terms of the Creative Commons Attribution License (http://creativecommons.org/licenses/by/4.0)